# Interactions among the Winter Monsoon, Ocean Eddy and Ocean Thermal Front in the South China Sea

Guihua Wang [1]

Jiaxun Li [2,1]

Chunzai Wang [3]

Yunwei Yan [1]

[1] State Key Laboratory of Satellite Ocean Environment Dynamics

Second Institute of Oceanography

Hangzhou, China

[2] Institute of Meteorology

PLA University of Science and Technology

Nanjing, China

[3] Physical Oceanography Division

NOAA/Atlantic Oceanographic and Meteorological Laboratory

Miami, Florida, USA.

## Abstract

[1] Sea surface temperature (SST) in boreal winter shows a robust feature of ocean front west of Luzon Island where a cyclonic ocean eddy is associated with the winter northeast monsoon. Our analyses further show that cold (warm) water is located in the northwest (southeast) part of the Luzon eddy due to ocean advection, forming the west Luzon front. The results suggest a novel mechanism of the positive feedback among the winter monsoon, ocean eddy and ocean front over the South China Sea. A strong positive wind stress curl associated with the winter monsoon and mountainous islands produces the Luzon eddy. The Luzon eddy is accompanied by negative (positive) SST anomalies in the northwest (southwest) part of the eddy, inducing the west Luzon thermal front. The SST anomalies can further force an anomalous wind pattern that converges onto the positive SST anomalies and diverges from the negative SST anomalies. The anomalous wind distribution in turn enhances the positive wind stress curl west of Luzon Island.



**Key words:** winter monsoon, ocean eddy, ocean thermal front, air-sea interactions

## 1. Introduction

[2] The South China Sea (SCS) is a unique semi-enclosed ocean basin surrounded by Asian continent, the Philippine Islands and Borneo Island (Figure 1). The upper layer ocean of the SCS is under the influence of the East Asian monsoon (Qu et al., 2000; Wang et al., 2009). The southwest summer monsoon occurs around middle May and prevails from June to August. The northeast winter monsoon first appears over northern part of the SCS in September, reaches the central SCS in October, covers the entire SCS in November, and then gradually diminishes in April. In winter, the northeast wind is strongly affected by the mountains over Taiwan Island and Luzon Island, producing a series of wind shears and wind stress curls with alternating signs from the north to the south (Wang et al., 2008).

[3] The large-scale ocean circulation in the SCS shows a robust seasonal cycle in response to the monsoon winds. In summer, the basin-scale circulation splits into a cyclonic gyre north of about 12°N and an anticyclonic gyre south of it, whereas the basin-scale circulation is generally cyclonic in winter (Liu et al., 2001). Embedded in the gyres are many mesoscale ocean eddies, as observed from multi-satellite data and hydrographic observations (Wang et al., 2003; Xiu et al., 2010). In summer, there is an eddy dipole off central Vietnam (Wang et al, 2006). In winter, along the eastern SCS is an alternating anticyclonic and cyclonic eddy pattern, which is associated with alternating wind stress curls there (Wang et al., 2008).

[4] Among these eddies, the west Luzon eddy exists at around 18°N, 118°E, with 200 km for the horizontal scale and 400 m for the vertical scale (Qu, 2000). The eddy appears in October, peaks from December to January, and decays after the monsoon reverse from winter

to summer. Climatological ocean temperature and altimetry data (Qu, 2000; Yang, 2000) shows that the eddy is quasi-steady. More and more evidences find that wind stress curl off northwest Luzon Island plays a major role in generating and maintaining the eddy (Wang et al., 2008). Some of previous studies called the cold eddy as mesoscale cyclonic circulation or a strong upwelling region. Although the estimated Rossby radius for the west Luzon is about 60-80 km, we still name the structure of about 200 km size as the 'west Luzon eddy' according to the traditional description.

[5] In addition, both the SCS SST and fronts have been widely studied with in situ observations, remote sensing data and model output (e.g., Chen et al., 1983; Li, 1996; Li et al., 2000; Wang et al., 2001; Belkin and Cornillon, 2003; Hu et al., 2003; Liu et al., 2005). The SCS is generally colder than the eastern Indian Ocean or the western Pacific Ocean in winter although it is located in the area of the Indo-Pacific warm pool (Figure 1, also see Liu et al., 2004). The SST in winter is generally warm in the southeastern SCS and cold in the northwestern SCS, thus the SST contours have a SW-NE orientation (from the southwest to northeast). The SST contours become denser distinctly west of Luzon Island, and front activity is stronger over there (Figure 1). As shown in Fig. 1, the isotherm of 27°C SST contour is located near the middle of the front.

[6] As discussed above, a strong monsoon wind shear, a quasi-steady cyclonic eddy and a thermal front appear in the west of Luzon Island at the same time during winter (Figure 2). To our knowledge, the linkages or potential interactions among these three features are unknown. The present study first examines variability of the west Luzon front and its mechanism, and then investigates the linkages among the west Luzon ocean front, west

84 Luzon ocean eddy and monsoon wind. Based on the observations and an ideal model, we
85 propose a novel feedback mechanism among the winter monsoon, ocean eddy and ocean
86 front.
87
88 **2. Data Sets**
89 [7] The SST data set from January 2006 to December 2010 is produced by the Remote
90 Sensing Systems (REMSS). It is a merged SST product measured by both the infrared
91 sensors from Moderate Resolution Imaging Spectroradiometer (MODIS) and microwave
92 sensors from Advanced Microwave Scanning Radiometer for Earth Observing System
93 (AMSR-E) and Tropical Rainfall Measuring Mission (TRMM) Microwave Images (TMI).
94 The former is high resolution but seriously impacted by cloud contamination, while the latter
95 has through-cloud capabilities but with a coarse resolution. All gaps are filled using optimum
96 interpolation method (Reynolds and Smith, 1994). The spatial resolution of this product is
97 about 9 km, and temporal sampling frequency is daily, which can well resolve ocean fronts
98 and eddies. The air temperature is from the Atmospheric Infrared Sounder (AIRS), which can
99 provide a three-dimensional view of the troposphere over the global ocean. The product has
100 24 vertical levels on a 1° horizontal grid. Monthly surface heat flux data on 1° grid is from
101 the Objectively Analyzed air-sea Fluxes (OAFlux) produced by the Woods Hole
102 Oceanographic Institution (WHOI).
103 [8] The sea surface height anomaly (SSHA) is a combined data product from
104 TOPEX/Poseidon (T/P), European Remote Sensing (ERS) and Jason-1 satellites. The SSHA
105 is calculated with respect to 13 year mean (January 1993 to December 2005) and mapped on

106 a global irregular grid about 1/3 degree spacing. The data from January 1993 to December
107 2010 are obtained from the AVISO (Archiving, Validation and Interpretation of Satellite
108 Oceanographic data) and monthly data were averaged to construct monthly climatology.

109 [9] The QuikSCAT wind data set from January 2000 to December 2008 comes from the
110 observations by the SeaWinds scatterometer on the Quick Scatterometer space mission of the
111 National Aeronautics and Space Administration (NASA). The wind is one of the
112 best-resolved products available. The temporal resolution is 1 day and the spatial resolution is
113 0.25° latitude × 0.25° longitude.

114 [10] The monthly climatology of observed temperature and salinity from U.S. Navy
115 Generalized Digital Environment Model (GDEM-Version 3.0) is used to identify the vertical
116 structure of the west Luzon front. It has a horizontal resolution of 0.25° latitude × 0.25°
117 longitude, and 78 standard depths from the surface to 6600 m with a vertical resolution
118 varying from 2 m at the surface to 200 m below 1600 m. The data evaluation for the global
119 oceans was reported by Carnes (2009), demonstrating that the GDEM is able to capture some
120 detailed front structures.

121

122 **3. Results**

123 **3.1 Observation and mechanism of west Luzon front**

124 [11] The ocean thermal front off west Luzon Island was observed by REMSS frequently.
125 Figures 3a and 3b show the front on January 7, 2006 and December 7, 2007, respectively. We
126 can see the front extends southeastward to around 114°E, 15°N. The fronts have large spatial
127 and temporal variability observed from daily images. To get a stable statistical distribution of

ocean fronts, we calculate the 5-year probability of fronts in the northern SCS. The probability is defined as the number of pixels that contain a front dividing by the total number (Hickox et al., 2000). The front threshold is that horizontal SST gradient is larger than 0.04 °C/10 km. In addition to the evident thermal front along the Guangdong coast, the west Luzon front is also apparent in the probability image (Figure 2). Generally, the front pattern in the probability image is quite similar to the climatology of front intensity distribution in Figure 1. The front extends to the southwest beyond 114°E/16°N from northern tip offshore of Luzon Island. It is the strongest around the box at 119-120.5°E, 17.5-19.0°N (see Figure 2), where the front probability is also the largest.

[12] Figure 2 also shows that the west Luzon front is exactly surrounded by the Luzon eddy, which can be well defined by the contour of -4 cm in the SSHA map. It is noted that the front is the strongest almost in the core of the Luzon eddy. To further investigate the linkage between the Luzon front and the Luzon eddy, we also calculate the front intensity and the SSHA at the box of 119-120.5°E, 17.5-19.0°N from October to next May as shown in Figure 4. The front appears in October, then develops from November to January, peaks around January-February, decays from February to May progressively, and disappears in summer. The horizontal gradient for the surface front has a maximum value of 0.19 °C/10 km in January and February. Figure 4 also shows that the Luzon cyclonic eddy appears in November, reaches its maximum strength in January-February, and decays after May, consistent with the variation of front intensity. Figures 5b and 5c further show the time-latitude diagrams along 119.5°E from 2006 to 2008. The time-latitude diagram shows that the evolution of the Luzon eddy is consistent with the evolution of front intensity. The

correlation coefficient between them can reach 0.78 (Figure 5d), which is significant at 95% confidence level. The evolution of the SSHA also reveals that the Luzon eddy is quite standing (Figure 5b).

[13] The above results suggest that the Luzon eddy may play an important role for the formation of the west Luzon front. To examine whether and how the Luzon eddy affects the front structure, we apply a simple mixed layer temperature equation to estimate the SST change due to the Luzon eddy (Qu, 2001):

$$\frac{\partial T}{\partial t} = \underbrace{-(u_g + u_e)\frac{\partial T}{\partial x} - (v_g + v_e)\frac{\partial T}{\partial y}}_{\text{(a)}} + \underbrace{\frac{Q}{\rho C_p h_m}}_{\text{(b)}} - \underbrace{\frac{W_{ent}(T - T_d)}{h_m}}_{\text{(c)}} \qquad (1)$$

where T is the SST or the mixed layer temperature, and t is the time, x and y are the conventional Cartesian coordinates, $u_g$ ($u_e$) and $v_g$ ($v_e$) are the geostrophic (Ekman) components of ocean velocity corresponding to x and y, respectively. Q is the net surface heat flux, $C_p$ is the specific heat capacity per unit volume. $h_m$ is the mixed layer depth, $\rho$ is the reference density of seawater, $W_{ent}$ is the entrainment velocity, $T_d$ is the water temperature at a depth of 5 m below the base of mixed layer. The terms in the right hand side of equation (1) are called horizontal the heat advection term (a), net heat flux (b) and vertical heat entrainment (c), respectively. The heat advection term includes the Ekman heat advection and geostrophic heat advection.

[14] The contributions of the net heat flux, Ekman heat advection, vertical entrainment and their sum to the SST tendency in the winter are shown in Figure 6. The Ekman heat advection shows positive temperature tendency about 2-6 °C/month off the west Luzon Island. The horizontal Ekman heat advection and vertical entrainment are generally very

small. Compared the individual terms with the sum, the Ekman heat advection is a dominant term to change the SST. However, the warming effect of Ekman heat advection can't produce the thermal front pattern as shown in Figure 1, thus it is logically to suppose that the geostrophic heat advection should be important to produce the thermal front.

[15] To consider the geostrophic heat advection effect, we calculate $u_g$ and $v_g$ by using the thermal wind relation (the reference velocity is set to be 0 at 1000 m) with GDEM data. To further isolate the Luzon eddy effect, we divide the geostrophic current (Figure 7b) into two components by applying a 200-km spatial filter: One is for basin-scale (Figure 7d), which can be described as the large scale cyclonic circulation driven by the monsoon; and the other is for mesoscale associated with the Luzon eddy (Figure 7f). We take the zonal average of the SST as the initial SST distribution (Figure 7a), neglect the Ekman heat advection term, net heat flux and vertical heat entrainment, and then integrate Equation (1).

[16] For the case of the basin scale circulation, the simulated SST pattern and the basin scale current do not show the thermal front off west Luzon island (Figures 7c and 7d), indicating the basin scale circulation is not responsible for the thermal front formation. However, the simulated SST pattern and the west Luzon front (Figures 7e and 7f) with the mesoscale current are generally quite similar to the observation (Figure 1), although they have some differences in details. The simulated SST contours also extend to the northeast from the southwest. The simulated SST is also warm in the southeastern SCS and cold in the northwestern SCS. Specifically, the SST contours become denser in the west of Luzon Island. The simulated west Luzon front is exactly corresponded to the regime of the Luzon eddy (Figure 7f). The model result indicates that the heat advection by the Luzon eddy is very

important for the formation of the west Luzon front. The dynamical linkage between the front and Luzon eddy can be summarized as follows. The northwest of the Luzon cyclonic ocean eddy is associated with the southwestward current, which advects the cold water from the northeast to the southwest, while the eddy advects the warm water from the southwest to the northeast in its southeast part because of the northeastward current. Thus, the west Luzon front is formed due to the ocean heat advection difference between the southeast part and the northwest part of the Luzon eddy.

### 3.2 Air-sea interactions in the northwest of Luzon Island

[17] Air-sea interactions over ocean fronts and eddies have been studied previously (Xie et al., 2001; Small et al., 2008), but the question is: are there any air-sea interactions associated with the west Luzon front and eddy? The west Luzon ocean front is also clearly seen in the vertical ocean temperature structures (Figure 8). The gridded ocean temperature data from GDEM demonstrate that the west Luzon ocean front is almost uniform vertically from the surface to the ocean mixed layer. The air temperature data from AIRS also show that there is an atmosphere front. The atmosphere front is located north of the ocean surface front and tilts northward with height (Figure 8). The co-existence of the ocean and atmosphere fronts suggests that the ocean interacts with the atmosphere in this area.

[18] The northeast monsoon winds over the SCS in winter are blocked and redirected by the mountains over Taiwan Island and Luzon Island, while became narrow and intense through the gaps of the mountain ranges like Luzon Strait. Associated with the wind shear pattern, the region west of Luzon Island is covered with a strong positive wind stress curl,

which is the main forcing to produce the Luzon eddy. Both Figure 4 and Figure 5d show that the wind stress curl and the Luzon eddy have a good correlation. Furthermore, the Luzon eddy usually lags the wind stress curl by about one month. This is roughly the time that the direct wind forcing spins up an eddy (Wang et al., 2008).

[19] Here we apply a 4° moving average in the meridional direction for SST field for the purpose of removing the monsoon background state to highlight the island wake (Figure 9). There are a series of SST anomalies with alternating signs from the north to the south. All of them slant toward the southwest beginning from the eastern boundary of the SCS. The bands of negative and positive SST anomalies off northwest Luzon Island tilts toward the southwest from 120.5°E to 116.0°E. Comparing SST anomalies and SSHA in Figure 9, we see that the negative and positive SST anomalies correspond to the northwest and southwest part of the Luzon eddy, respectively. Again, the good correlation (the maximum correlation coefficient can reach 0.79) indicates that the eddy plays an important role in regulating the SST anomalies. Figure 5e also shows that there is almost no time lag between the thermal front and the Luzon eddy. Our simulation also shows that it usually takes 1-2 weeks for the temperature adjustment to reach the equilibrium state if the ocean is forced by the mesoscale heat advection. Thus, the temperature adjustment to the eddy heat advection is very fast.

[20] Wind vectors in Figure 9 also show that the anomalous winds converge onto the warm water band and diverge from the cold water. The observed SST-induced anomalous wind is mainly attributable to stability changes of the atmospheric boundary layer. The mechanism has been observed and simulated in many regions (Chelton and Xie, 2010). The anomalous winds in turn intensify the background northeast monsoon in the cold band, while

they weaken the northeast monsoon in the warm band. This results in a stronger positive wind stress curl, indicating that the ocean front can force the atmosphere.

[21] The results presented here suggest a positive feedback among the winter monsoon, Luzon ocean eddy and SST over the SCS. As the winter monsoon blows over the SCS, the northeast wind is intensified through Luzon strait and weakened after the mountains of Luzon Island, forming a positive wind stress curl west of Luzon Island. The positive wind stress curl produces the Luzon cyclonic ocean eddy. In the northwest of the Luzon cyclonic eddy the cold water is advected from the northeast to the southwest, while in the southeast part of the eddy the warm water is advected from the southwest to the northeast, thus resulting in the west Luzon front (negative and positive SST anomalies in the northwest and southeast part of the Luzon eddy, respectively). Then the anomalous winds converge onto the positive SST anomalies and diverge from the negative SST anomalies. This anomaly wind distribution intensifies the background northeast monsoon in the northwest of the Luzon eddy and weakens the monsoon wind in the southeast of the Luzon eddy, which in turn enhance the positive wind stress curl west of Luzon Island.

## 4. Summary

[22] The ocean front in the west of Luzon Island is investigated by using a suite of satellite measurements and an ideal temperature equation. The ocean front only occurs during in winter because of the winter northeast monsoon. The ocean front is surrounded by the Luzon cyclonic ocean eddy and the front is the strongest almost in the core of the Luzon eddy. The gridded temperature data from Generalized Digital Environment Model (GDEM-Version

3.0) also demonstrate that the west Luzon ocean front exists from the surface to the mixed layer. Our results show that the formation of the west Luzon front is strongly associated with the Luzon eddy. The Luzon cyclonic eddy advects the cold water from the northeast to the southwest and the warm water from the southwest to the northeast in its northwest and southeast part, respectively. The advected warm and cold water further results in the west Luzon front.

[23] Based on these results, we further propose a positive feedback among the winter monsoon, ocean eddy and sea surface temperature. In winter, a positive wind stress curl west of Luzon Island is associated with the northeast winter monsoon and the mountainous island chain. Forced by the positive wind stress curl, a strong cyclonic eddy is formed in west Luzon. Because cold (warm) water is advected from the northeast to the southwest (the southwest to the northeast), the negative (positive) SST anomalies appear in the northwest (southeast) part of the Luzon eddy. The negative (positive) SST anomalies can further force an anomalous wind pattern that converges onto the positive SST anomalies and diverges from the negative SST anomalies. The anomalous wind distribution in turn enhances the positive wind stress curl west of Luzon Island.

[24] **Acknowledgements.** The study was supported by the National Natural Science Foundation of China (Grant No. 41125019 and 40976017) and the Foundation for Innovative Research Groups of the Natural Science Foundation of Zhejiang (Grant No.2009R50044 ).

281 **References**


282 Belkin, I., and P. Cornillon (2003), SST Fronts of the Pacific Coastal and Marginal Seas,
283 Pacific Ocean, *Pacific Oceanogr.*, 1, 90-100.

284 Canes, M. R. (2009), Description and evaluation of GDEM-V3.0, *NRL Rep.*
285 *NRL/MR/7330-09-9165*, Nav. Res. Lab., Washington, D. C.

286 Chelton, D. B., and S.-P. Xie. (2010), Coupled ocean-atmosphere interaction at oceanic
287 mesoscales, *Oceanography*, 23(4), 52–69.

288 Chen, J. (1983), Some explanations for the real-time distribution of sea surface temperature
289 in the northern South China Sea in winter, *Acta Oceanol. Sin.*, 5(3), 391–395.

290 Hickox, R., I. Belkin, P. Cornillon, Z. Shan (2000), Climatology and seasonal variability of
291 ocean fronts in the East China, Yellow and Bohai Seas from satellite SST data, *Geophys.*
292 *Res. Lett.*, 27(18), 2945–2948.

293 Hu, J. Y., H. Kawamura, and D. L. Tang (2003), Tidal front around the Hainan Island,
294 northwest of the South China Sea, *J. Geophys. Res.*, 108(C11), 3342,
295 doi:10.1029/2003JC001883.

296 Li, L. (1996), Shelf/slope fronts in the northeastern South China Sea in March 1992, *Oceanic*
297 *Collection in China*, 6, 34–41.

298 Li, L., X. Guo, R. Wu (2000), Oceanic fronts in the southern Taiwan Strait, *J. Oceanogr.*
299 *Taiwan Strait*, 19(2), 147–156.

300 Liu, Q., X. Jiang, S.-P. Xie, and W. T. Liu (2004), A gap in the Indo-Pacific warm pool over
301 the South China Sea in boreal winter: Seasonal development and interannual variability,
302 *J. Geophys. Res.*, 109, C07012, doi:10.1029/2003JC002179.

303 Liu, Z. Y., H. J. Yang, Q. Y. Liu (2001), Regional Dynamics of Seasonal Variability in the
304 South China Sea, *J. Phys. Oceanogr.*, 31, 272–284.
305 Qu, T. D. (2000), Upper-Layer Circulation in the South China Sea, *J. Phys. Oceanogr.*, 30,
306 1450–1460.
307 Qu, T. D. (2001), Role of ocean dynamics in determing the mean seasonal cycle of the South
308 China Sea surface temperature, *J. Geophys. Res.*, 106(C4), 6943-6955.
309 Reynolds, R.W. and T.M. Smith (1994), Improved global sea surface temperature analyses
310 using optimum interpolation, *J. Climate*, 7, 929-948.
311 Small, R. J., S.P. de Szoeke, S.-P. Xie, L. O'Neill, H. Seo, Q. Song, P. Cornillon, M. Spall,
312 and S. Minobe (2008), Air-sea interaction over ocean fronts and eddies. *Dyn. Atmos.*
313 *Oceans*., 45, 274–319.
314 Wang, B., F. Huang, Z. Wu, J. Yang, X. Fu, and K. Kikuchi (2009), Multi-scale climate
315 variability of the South China Sea monsoon: A review, *Dyn. Atmos. Oceans*., 47, 15-37.
316 Wang, G., J. Su, and P. C. Chu (2003), Mesoscale eddies in the South China Sea observed
317 with altimeter data, *Geophys. Res. Lett.*, 30(21), 2121, doi:10.1029/2003GL018532.
318 Wang, G., D. Chen, and J. Su (2006), Generation and life cycle of the dipole in the South
319 China Sea summer circulation, *J. Geophys. Res.*, 111, C06002,
320 doi:10.1029/2005JC003314.
321 Wang G., D. Chen and J. Su (2008), Winter eddy genesis in the eastern South China Sea due
322 to orographic wind-Jets, *J. Phys. Oceanogr.*, 38, 726-732.
323 Wang, D., Y. Liu, Y. Qi, and P. Shi (2001), Seasonal variability of thermal fronts in the
324 northern South China Sea from satellite data, *Geophys. Res. Lett.*, 28(20), 3963-3966.

325 Xie, S.-P., W. T. Liu, Q. Liu, and M. Nonaka (2001): Far-reaching effects of the Hawaiian
326 Islands on the Pacific Ocean-Atmosphere, *Science*, 292, 2057–2060.
327 Xiu, P., F. Chai, L. Shi, H. Xue, and Y. Chao (2010), A census of eddy activities in the South
328 China Sea during 1993-2007, *J. Geophys. R*es., 115, C03012,
329 doi:10.1029/2009JC005657.
330 Yang, H. J., Simulation of the circulation of the South China Sea (in Chinese), Ph.D. thesis,
331 China Ocean Univ., Qingdao, China, 2000.
332

## Figure Captions

**Figure 1.** Winter sea surface temperature (with contour interval of 1 °C; shaded in pink for SST ≥28 °C) and front intensity (°C/10km, in color). TI: Taiwan Island; LI: Luzon Island: HI: Hainan Island. The inserted box (111-121°E, 13-23°N) is the study zone plotted in most figures.

**Figure 2.** Winter sea surface height anomaly (cm, in contour), front probabilities (in color) and wind vector (m/s) in the South China Sea. Solid (dashed) lines represent positive (negative) values of sea surface height anomaly, and the land topography with elevations greater than 500 m is shaded in black. The inserted box (119-120.5°E, 17.5-19°N) is the front where the probability is the largest.

**Figure 3.** Sea surface temperature (°C, in contour), front intensity (°C/10 km, in color) and ocean current (cm/s) in the South China Sea on (a) January 7, 2006 and (b) December 7, 2007. The pink dashed line indicates the -4 cm contour of sea surface height anomaly.

**Figure 4.** Seasonal variability of west Luzon front intensity (°C/10 km, in black), sea surface height anomaly (cm, in red) and wind stress curl ($10^{-7}$ N $m^{-3}$ in blue).

**Figure 5.** Time-latitude diagrams of (a) wind stress curl ($10^{-7}$ N $m^{-3}$), (b) sea surface height anomaly (cm), and (c) front intensity (°C/10 km) along 119.5°E. Shown in (d) is the

correlation between wind stress curl and sea surface height anomaly, and (e) is the correlation between sea surface height anomaly and front intensity.

**Figure 6.** The heat budget in the northern South China Sea: (a) net heat flux term, (b) Ekman heat advection term, (c) vertical entrainment term, and (d) sum of (a), (b) and (c). Units are °C/month. The white dashed line is the contour of -4 cm in the SSHA, which represents the front position. In (b), the vector is the Ekman velocity.

**Figure 7.** (a) Ideal sea surface temperature distribution (°C); (b) geostrophic current from GDEM dataset; (c) and (e) are the sea surface temperature considering the advection effect by the basin scale circulation and mesoscale circulation, respectively; (d) and (f) are the front intensity (°C/10 km, in color) deduced from (c) and (e), respectively, and vectors are for basin scale and mesoscale circulation, respectively. In (f), solid (dashed) brown contours represent positive (negative) values of sea surface height anomaly.

**Figure 8.** Vertical atmosphere and ocean temperature distribution (°C, in contours) and front intensity (°C/10 km, in color) on the 119°E transect. The green-dashed line indicates the ocean mixed layer depth. The ocean and atmosphere temperatures are averaged for the winters from GDEM and AIRS, respectively.

**Figure 9.** High-pass filtered sea surface temperature (°C, in color) and wind vectors (m $s^{-1}$). The latitudinal filtering is done by subtracting a 4° moving average from the original

data to remove the large-scale monsoon background state. White contour is sea surface height anomaly (cm). Solid (dashed) white contours represent positive (negative) values of sea surface height anomaly.

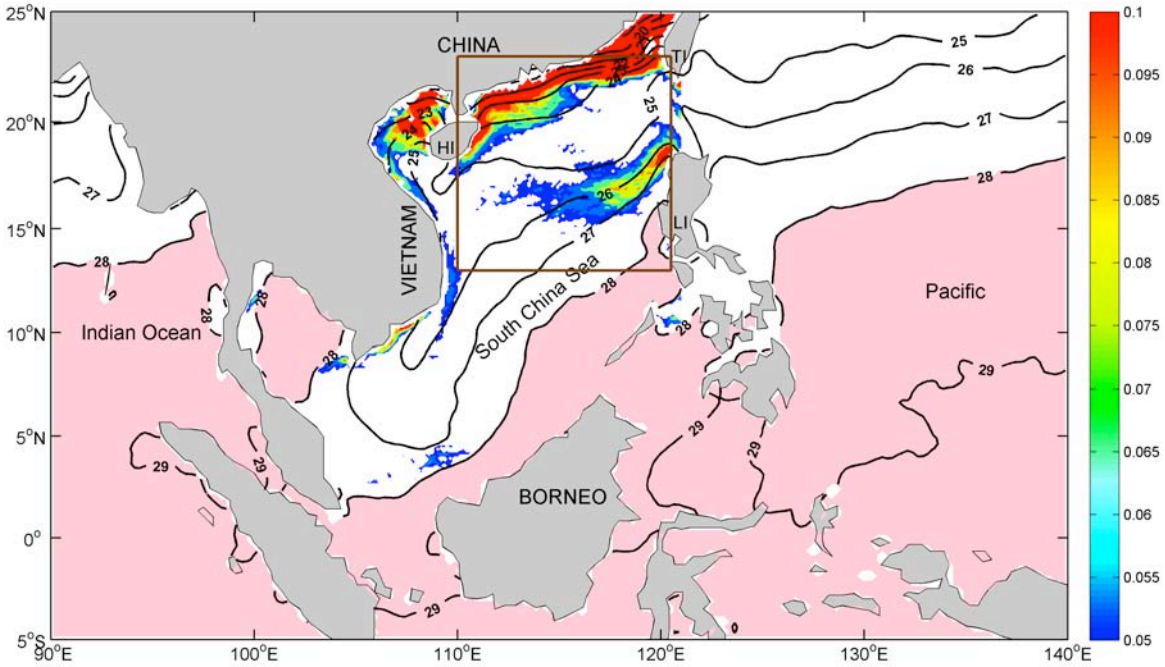


**Figure 1.** Winter sea surface temperature (contours at 1°C intervals; shaded in pink for SST ≥28 °C ) and front intensity (°C/10km, in color). TI: Taiwan Island; LI: Luzon Island: HI: Hainan Island. The inserted box (111-121°E, 13-23°N) is the study zone plotted in most figures.

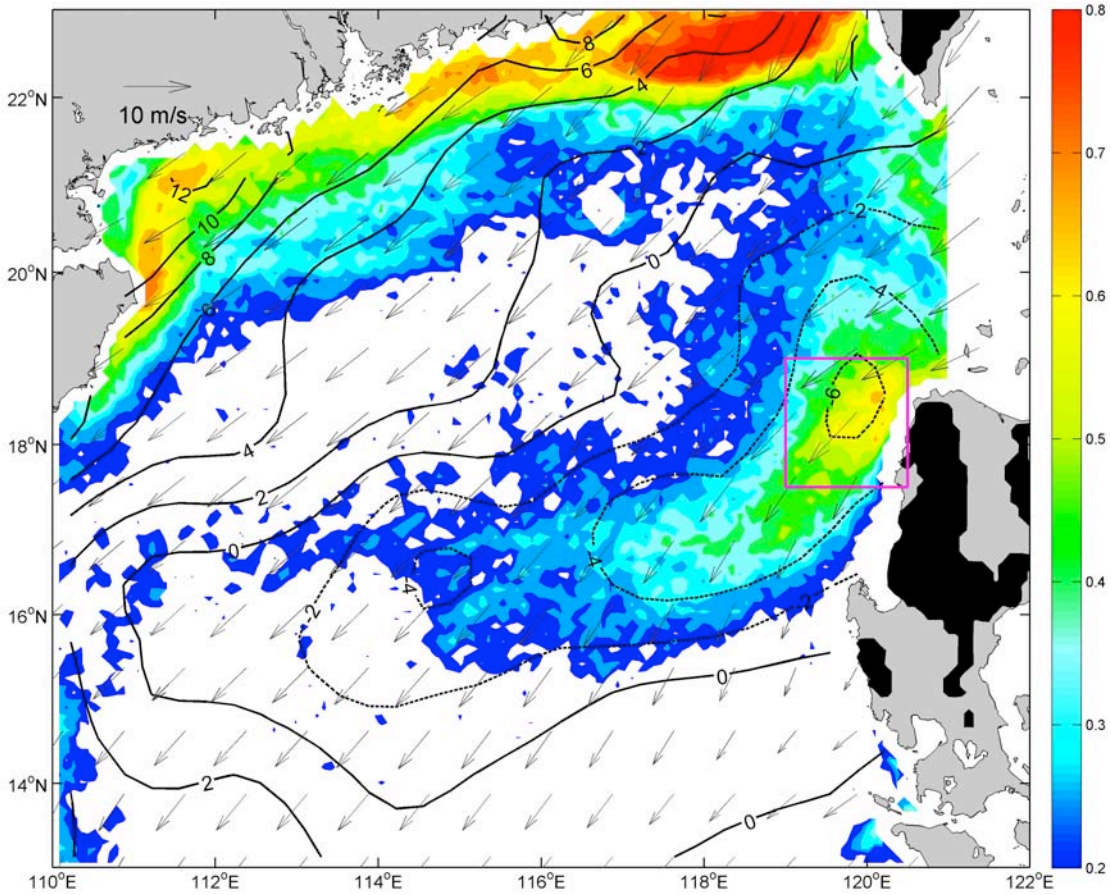


**Figure 2.** Winter sea surface height anomaly (cm, in contour), front probabilities (in color) and wind vector (m/s) in the South China Sea. Solid (dashed) lines represent positive (negative) values of sea surface height anomaly, and the land topography with elevations greater than 500 m is shaded in black. The inserted box (119-120.5°E, 17.5-19°N) is the front where the probability is the largest.

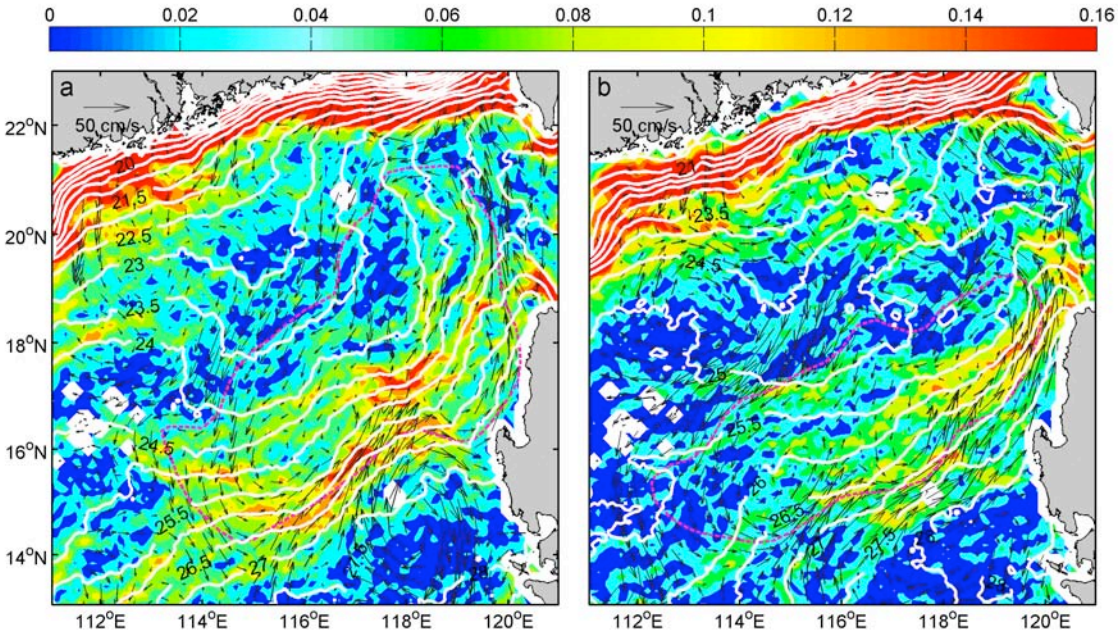


16

17 **Figure 3.** Sea surface temperature (°C, in contour), front intensity (°C/10km, in color) and

18 ocean current (cm/s) in the South China Sea on (a) January 7, 2006 and (b) December 7, 2007.

19 The pink dashed line indicates the -4 cm contour of sea surface height anomaly.

20

21

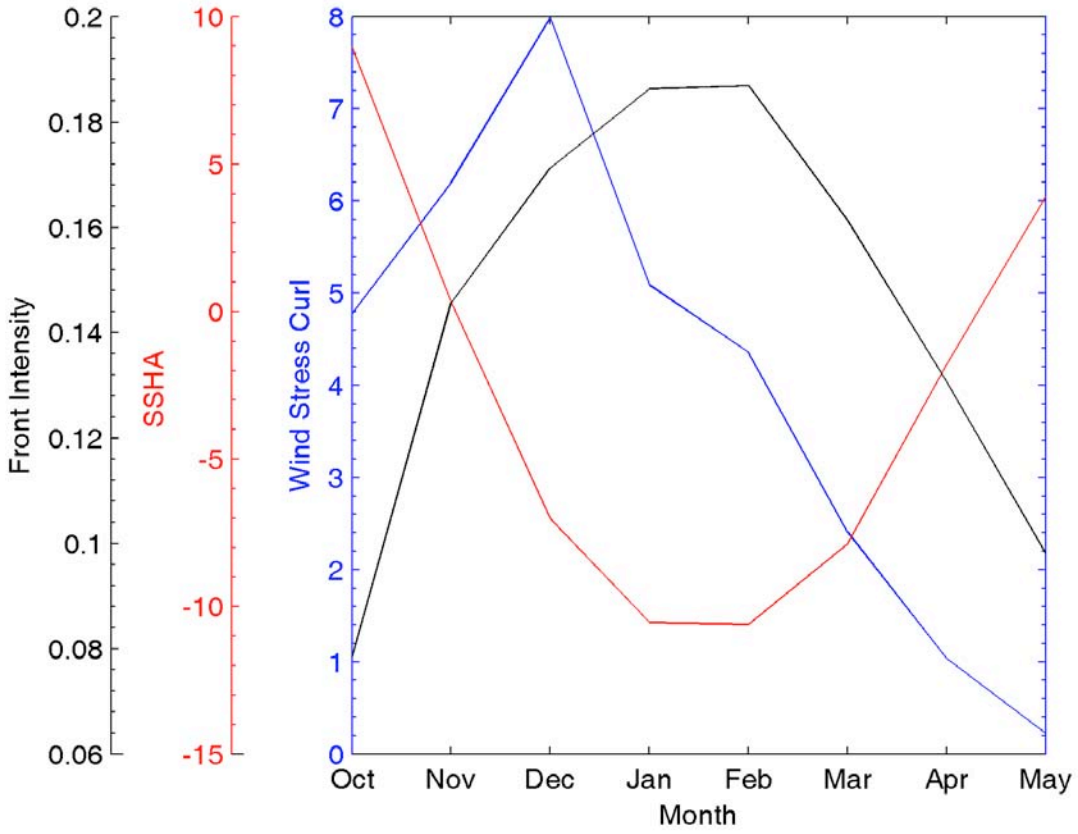


**Figure 4.** Seasonal variability of west Luzon front intensity ($^{o}$C/10 km, in black), sea surface height anomaly (cm, in red) and wind stress curl ($10^{-7}$ N m$^{-3}$ in blue).

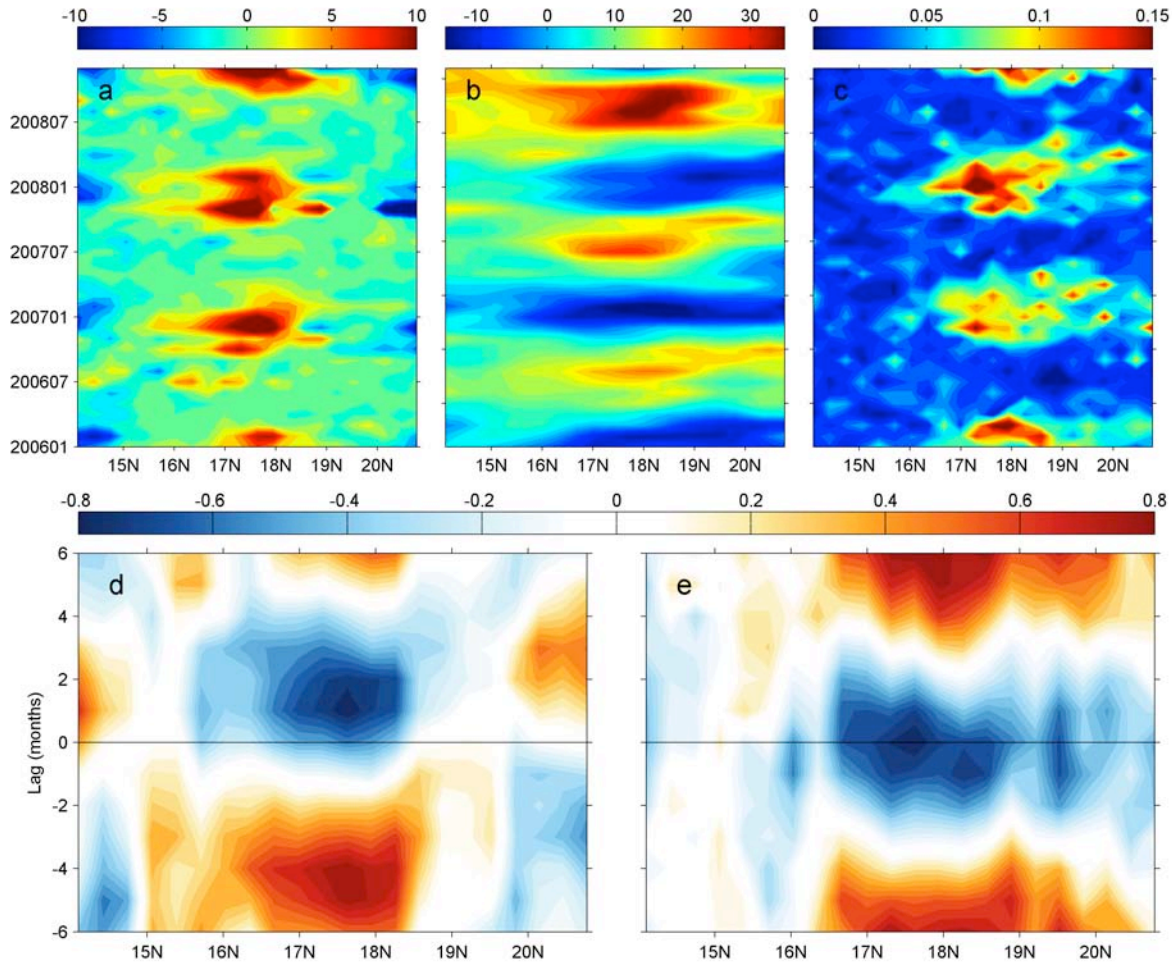


**Figure 5.** Time-latitude diagrams of (a) wind stress curl ($10^{-7}$ N $m^{-3}$); (b) sea surface height anomaly (cm); (c) front intensity ($^{o}$C/10 km) along 119.5$^{o}$E; (e) is the correlations between wind stress curl and sea surface height anomaly, and (f) is the correlations between sea surface height anomaly and front intensity.

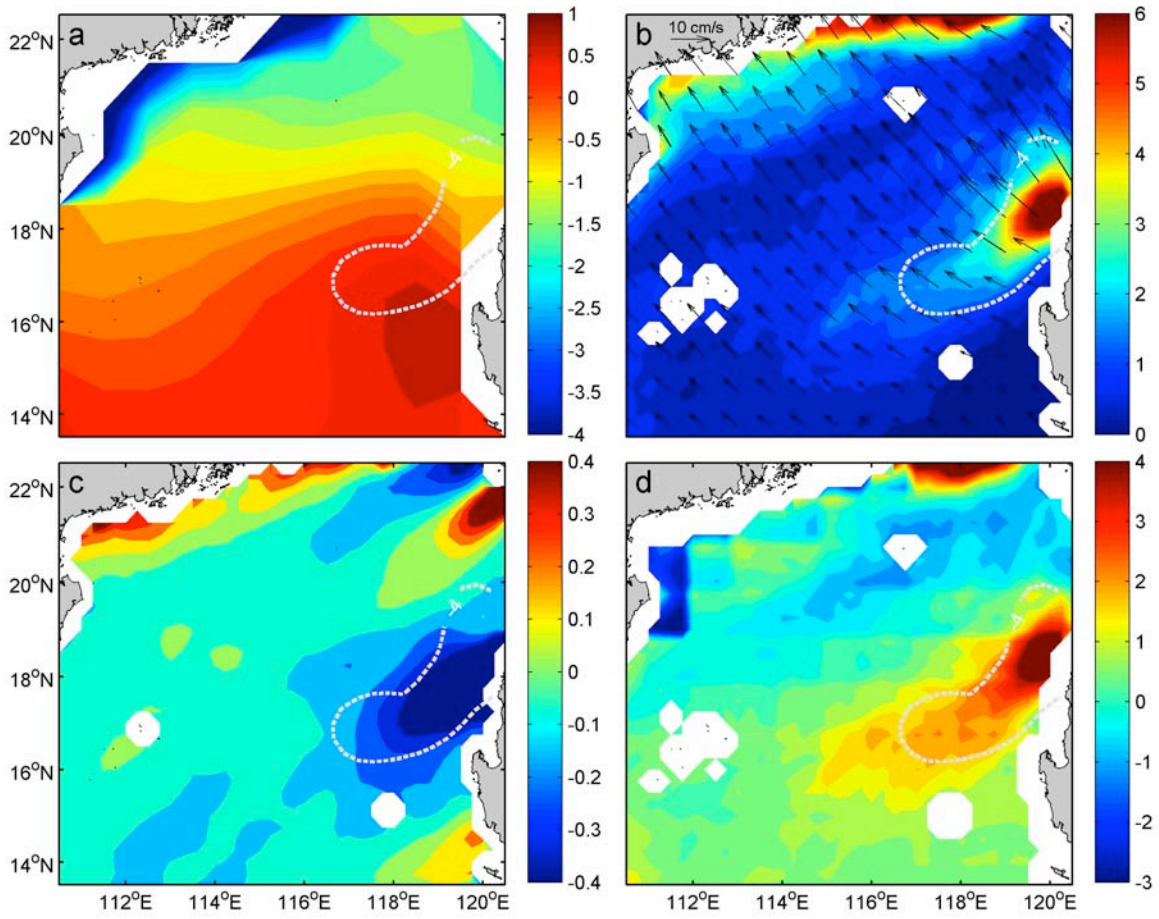


**Figure 6.** The heat budget in the northern South China Sea. (a) net heat flux term; (b) Ekman heat advection term; (c) vertical entrainment term and (d) sum of (a), (b) and (c). All the units are $^{o}$C/month. In (a)-(d), the white dashed line is the contour of -4 cm in the SSHA to present the front position. In (b), the vector is the Ekman velocity.

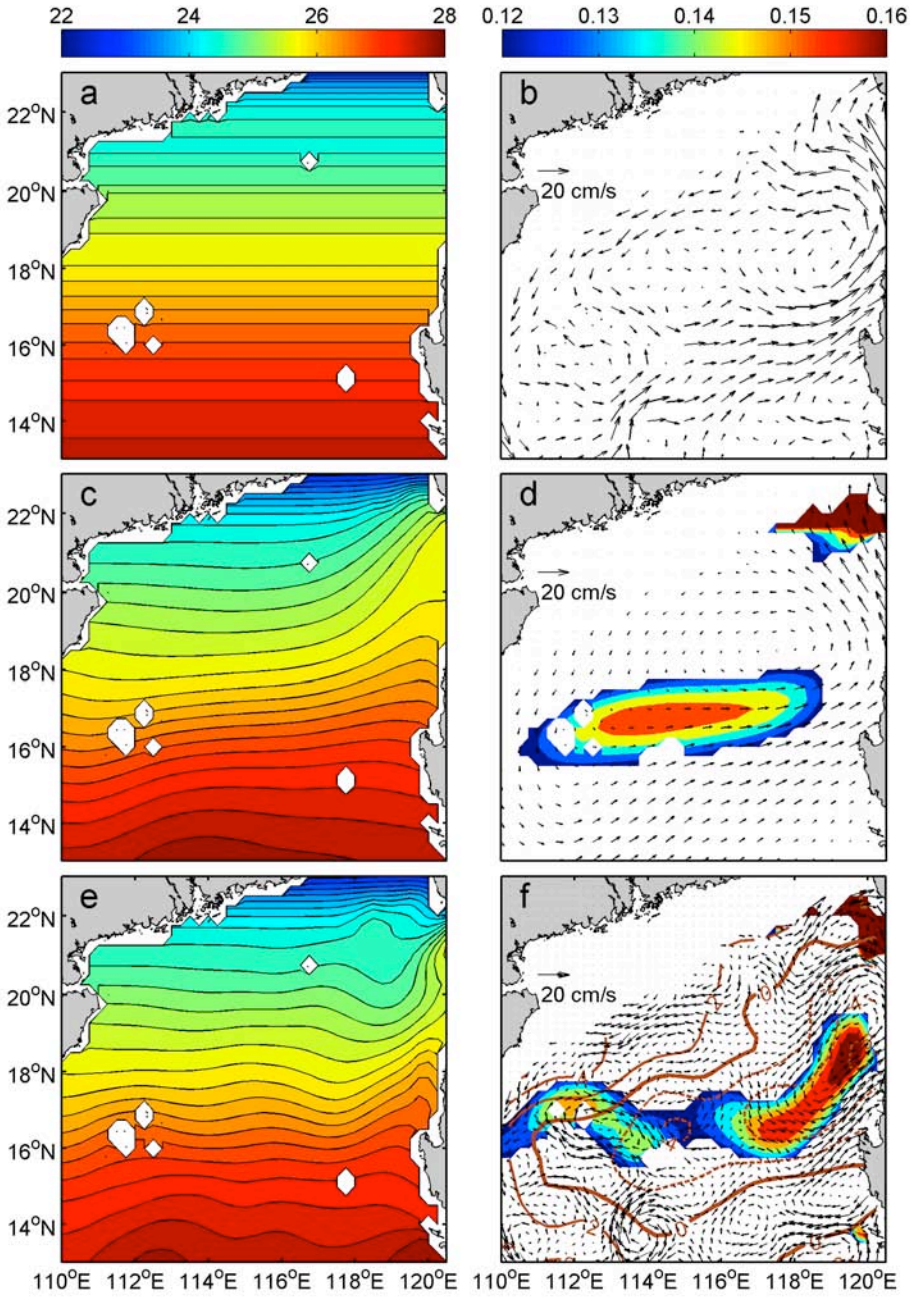


**Figure 7.** (a) Ideal sea surface temperature distribution (°C); (b) geostrophic current from GDEM dataset; (c) and (e) are the sea surface temperature considering the advection effect by the basin scale circulation and mesoscale circulation respectively; (d) and (f) are the front intensity (°C/10km, in color) deduced from (c) and (e) respectively, and vectors are for basin scale and mesoscale circulation accordingly. In (f), solid (dashed) brown contours represent positive (negative) values of sea surface height anomaly.

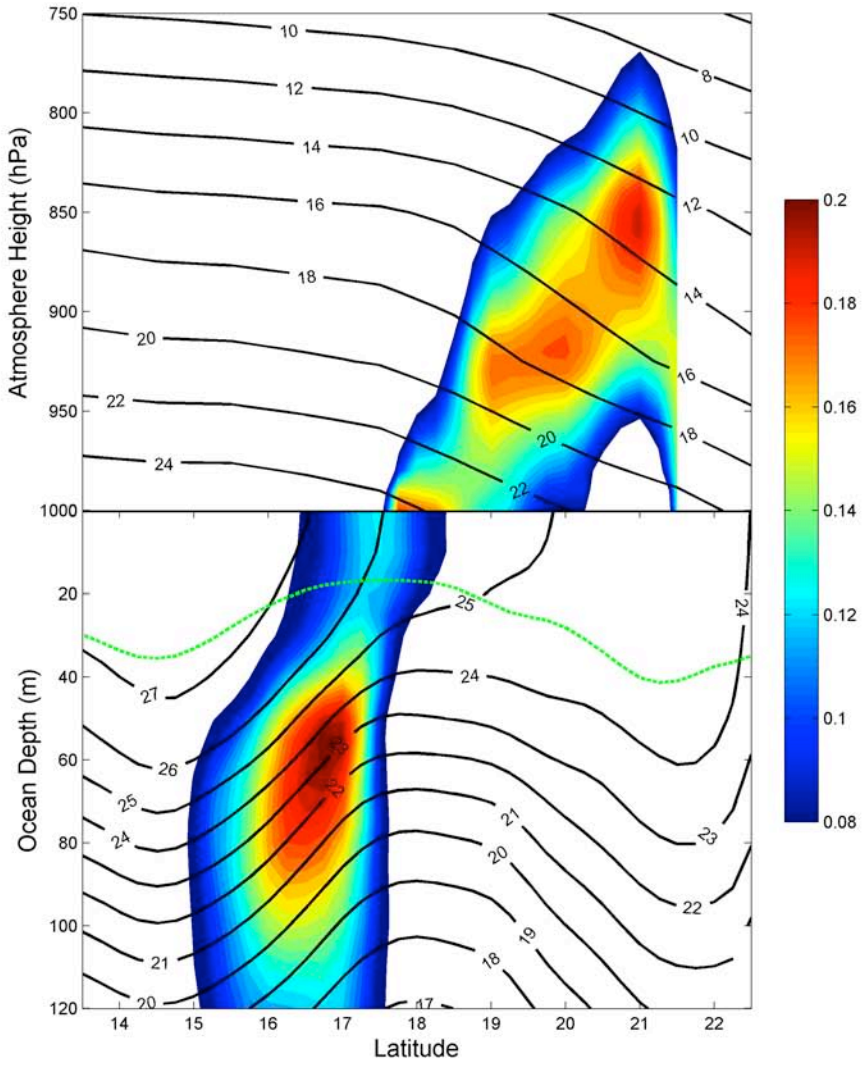


**Figure 8.** Vertical atmosphere and ocean temperature distribution ($^{o}$C, in contours) and front intensity ($^{o}$C/10km, in color) on the 119 $^{o}$E transect. The green-dashed line indicates the ocean mixed layer depth. Ocean and atmosphere temperatures are averaged for the winters from GDEM and AIRS, respectively.

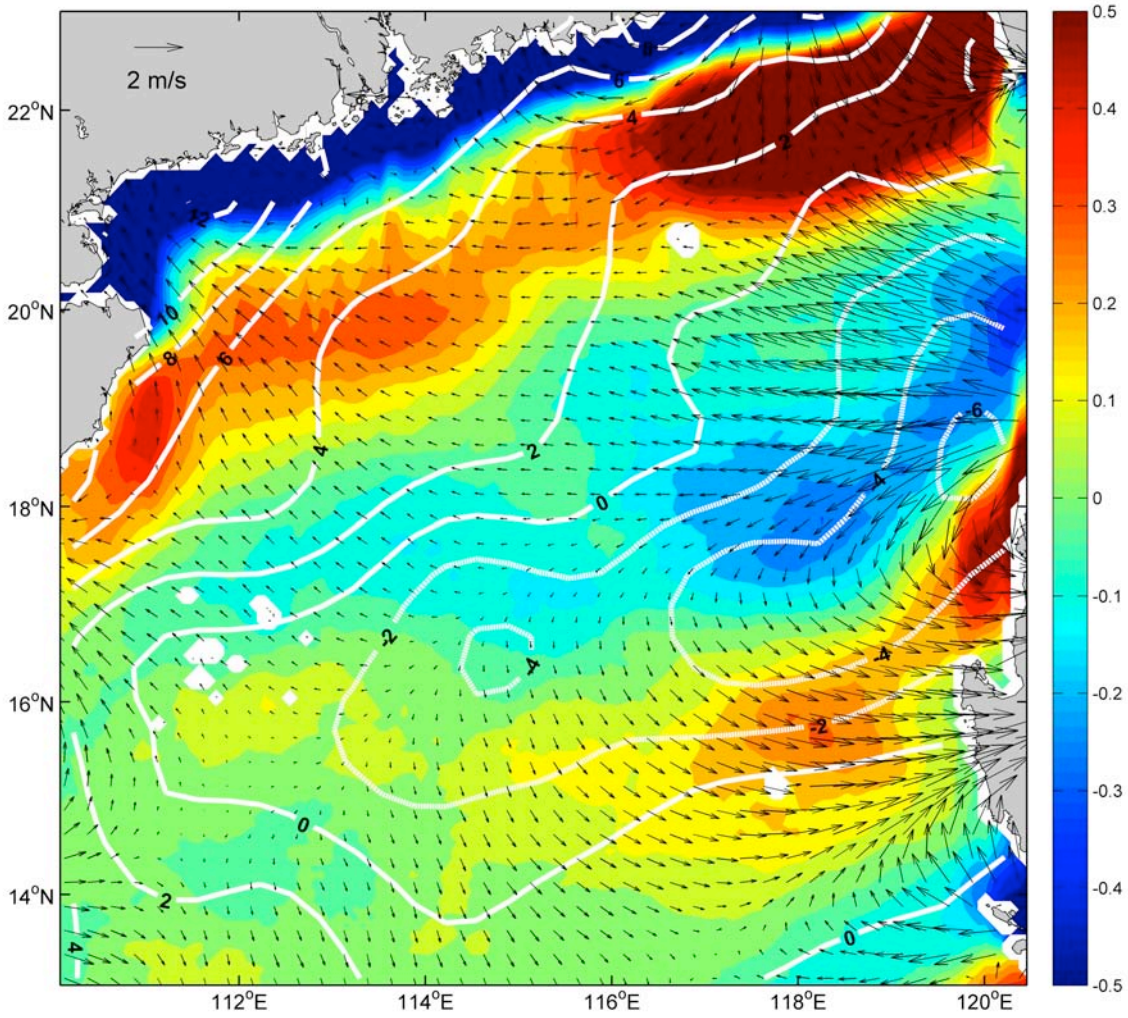


**Figure 9.** High-pass filtered sea surface temperature ($^{o}$C, in color) and wind vectors (m s$^{-1}$). The latitudinal filtering is done by subtracting a 4$^{o}$ moving average from the original data to remove the large-scale monsoon background. White contour is sea surface height anomaly (cm). Solid (dashed) white contours represent positive (negative) values of sea surface height anomaly.